Published in final edited form as:
Stem Cell Res. 2013 May ; 10(3): 267–277. doi:10.1016/j.scr.2012.12.006.

Migration of CD11b+ Accessory Cells During Murine Lung Regeneration

Kenji Chamoto[a], **Barry C. Gibney**[a], **Grace S. Lee**[a], **Maximilian Ackermann**[b], **Moritz A. Konerding**[b], **Akira Tsuda**[c], and **Steven J. Mentzer**[a]

[a]Laboratory of Adaptive and Regenerative Biology, Brigham & Women's Hospital, Harvard Medical School, Boston MA

[b]Institute of Functional and Clinical Anatomy, University Medical Center of Johannes Gutenberg-University, Mainz, Germany

[c]Molecular and Integrative Physiological Sciences, Harvard School of Public Health, Boston, MA

Abstract

In many mammalian species, the removal of one lung leads to growth of the remaining lung to near-baseline levels. In studying post-pneumonectomy mice, we used morphometric measures to demonstrate neoalveolarization within 21 days of pneumonectomy. Of note, the detailed histology during this period demonstrated no significant pulmonary inflammation. To identify occult blood-borne cells, we used a parabiotic model (wild-type/GFP) of post-pneumonectomy lung growth. Flow cytometry of post-pneumonectomy lung digests demonstrated a rapid increase in the number of cells expressing the hematopoietic membrane molecule CD11b; 64.5% of the entire GFP^+ population were $CD11b^+$. Fluorescence microscopy demonstrated that the $CD11b^+$ peripheral blood cells migrated into both the interstitial tissue and alveolar airspace compartments. Pneumonectomy in mice deficient in CD11b ($CD18^{-/-}$ mutants) demonstrated near-absent leukocyte migration into the airspace compartment ($p<.001$) and impaired lung growth as demonstrated by lung weight ($p<.05$) and lung volume ($p<.05$). Transcriptional activity of the partitioned $CD11b^+$ cells demonstrated significantly increased transcription of *Angpt1, Il1b,* and *Mmp8, Mmp9, Ncam1, Sele, Sell, Selp* in the alveolar airspace and *Adamts2, Ecm1, Egf, Mmp7, Npr1*, *Tgfb2* in the interstitial tissue (>4-fold regulation; $p<.05$). These data suggest that blood-borne $CD11b^+$ cells represent a population of accessory cells contributing to post-pneumonectomy lung growth.

Keywords

lung regeneration; parabiotic mice; hematopoietic $CD11b^+$ cells

Introduction

Post-pneumonectomy lung growth is a striking example of adult tissue morphogenesis. In many mammalian species, including humans (Butler et al., 2012; Kajstura et al., 2011),

Correspondence: Dr. Steven J. Mentzer, Room 259, Brigham &Women's Hospital, 75 Francis Street, Boston, MA 02115, smentzer@partners.org.

removal of one lung is associated with compensatory growth of the remaining lung to near-baseline levels (Hsia et al., 2004). In rodents, the growth occurs within days of pneumonectomy (Konerding et al., 2012). Recent studies have demonstrated that the growth of the remaining lung reflects not simply an increase in alveolar size, but an increase in the number of alveoli (Fehrenbach et al., 2008). Although the consequences of this process have been well-documented (Hsia et al., 2004), the mechanism of compensatory lung growth is unknown

In many organs, regeneration depends upon not only progenitor cells, but a microenvironment conducive to tissue growth (Nystul & Spradling, 2006; Scadden, 2006). These microenvironments—commonly referred to as “niches”—include the stromal structures and intercellular signals necessary to provide growth support. In the lung, a unique structural feature is that 90% of the organ volume is air. The alveolus, the gas exchange unit of the lung, is a small cavity surrounded by a thin epithelial lining and a delicate meshwork of capillaries. Because gas diffusion and exchange is sensitive to structural barriers, there are few stromal elements available to contribute to lung growth. Given the dramatic post-pneumonectomy growth in species such as the mouse, and the limited cellular diversity within the normal lung, it is likely that accessory cells, derived from the peripheral blood, contribute to the regenerative lung microenvironment.

Previous work from our laboratory has used a parabiotic cross-circulation model to identify blood-borne cells potentially contributing to post-pneumonectomy lung growth. Complete cross-circulation between wild-type (WT) and green fluorescent protein (GFP) parabionts results in 50% of the blood cells expressing GFP (Gibney, Chamoto, et al., 2012); these fluorescent cells can be tracked as they migrate into the remaining WT lung after pneumonectomy. This approach has demonstrated the migration and incorporation of $CD34^+$ progenitor cells into the growing lung microcirculation (Chamoto, Gibney, Lee, et al., 2012). Studies of alveolar macrophages ($CD11c^+$, $CD11b^-$) demonstrated few blood-derived cells—a finding consistent with local renewal (Chamoto, Gibney, Ackermann, et al., 2012). An intriguing observation in the flow cytometry studies of both alveolar macrophages and endothelial cells was a dominant population of blood-derived $CD11b^+$ cells within the growing lung. The $CD11b^+$ molecule, also known as MAC-1 or CR3, is natively expressed on a variety of lung cells including monocytes, small macrophages, dendritic cells, granulocytes and natural killer cells (Gonzalez-Juarrero, Shim, Kipnis, Junquieira-Kipnis, & Orme, 2003). CD11b is not typically expressed on the dominant leukocyte in the airspace (Matthews et al., 2007)—namely, alveolar macrophages. The rapid accumulation of the $CD11b^+$ population suggested a functional contribution of these cells to post-pneumonectomy lung growth.

In this report, we investigated the hypothesis that the normally scant stromal support for lung growth is augmented in post-pneumonectomy mice by blood-borne $CD11b^+$ cells. Although the CD11b marker was empirically identified, the CD11b membrane molecule defines a population of cells implicated in a variety of reparative and regenerative processes (Melero-Martin et al., 2010; Ohki et al., 2010). Relevant to the morphogenetic changes associated with interstitial capillary growth and alveolar epithelial growth, we anticipated that these blood-borne leukocytes could have an accessory role in lung regeneration.

Methods

Mice

Male mice, eight to ten week old wild type C57BL/6 (Jackson Laboratory, Bar Harbour, ME, USA) and CD18 hypomorphic mutant mice (B6.129S7-Itgb2^{tm1Bay}/J) (Jackson Laboratories) were used for nonparabiotic experiments. Wild-type and GFP^+ C57BL/6-Tg

(UBC-GFP) 30Scha/J (Jackson Laboratory) with similar age and weights were selected for parabiosis. The care of the animals was consistent with guidelines of the American Association for Accreditation of Laboratory Animal Care (Bethesda, MD, USA) and approved by our Institutional Animal Care and Use Committee.

Parabiotic surgery

The parabiotic experiments are outlined in the associated figure (Figure 1). The animals were paired based on a modified technique described by Bunster (Bunster & Meyer, 1933). Briefly, the animals were anesthetized with a intraperitoneal injection of ketamine 100 mg/kg (Fort Dodge Animal Health, Fort Dodge, IA, USA) and xylazine 10 mg/kg (Phoenix Scientific, St. Joseph, MO, USA). The right side of the wild type mouse and the left side of the GFP^+ mouse were surgically joined as previously described (Gibney, Chamoto, et al., 2012). Left pneumonectomy was performed 28 days after parabiosis.

Pneumonectomy

The animal was ventilated on a Flexivent (SciReq, Montreal, QC Canada) at ventilator settings of 200/min, 10 ml/kg, and PEEP of 2 cmH_2O with a pressure limited constant flow profile (Gibney et al., 2011). A thoracotomy was created in the left fifth intercostal space and a left pneumonectomy was performed by hilar ligation (Gibney, Houdek, et al., 2012). Postoperatively, the animal was removed from the ventilator and observed for spontaneous respirations. Once spontaneous muscle activity was noted, the animal was extubated. Sham thoracotomy—involving the same anesthesia, an identical incision and closure without surgical manipulation of the left lung—were included in each experimental condition. For the dependent measures in this study, there was no difference between sham thoracotomy and no-surgery controls.

Lung volumes and weights

After measurement of pulmonary mechanics, the animal was euthanized by exsanguination via the caval vein. The orotracheal tube was then connected to a 30 cmH_2O column of 2.5% buffered glutaraldehyde for 20 minutes, after which the trachea was ligated, and the lungs were dissected free from the chest. The lungs were then placed in cold 2.5% buffered glutaraldehyde for 24 hours, and then rinsed in two exchanges of cold PBS. Lung volume was determined by the water immersion method of Scherle (Yan, Carbayo, Weibel, & Hsia, 2003), and the lung subsequently embedded in paraffin. For measuring lung weights, blood-free wet lung was used after the exsanguination.

Histology

The paraffin embedded lungs were used for histologic section. Briefly, after a random start, 5um lung sections were obtained at 2mm intervals. The sections were deparaffinized and placed in a solution of 96% alcohol and 0.1% Sirius red/Picrid acid (Chroma F3BA, Fuerstenfeldbruck, Germany) for 30 min. After rinsing in distilled water, the sections were serially dehydrated in 80%, 96% and 98% alcohol. A final rinse with Xylol was performed before the slide is covered with Entellan.

Mean linear intercept (MLI)

Mean linear intercept (MLI) was measured using isotropic, uniform and random sampling. After randomly orienting the slides, the images were obtained with a JVC CCD-Digital Camera (Model KY-F-75U) attached to a Zeiss Axiophot microscope with a polarizing filter placed in the light path and processed with standard MetaMorph 7.5 (Molecular Devices, Brandywine, PA, USA). The lung parenchyma was thresholded, and a grid of 8 bars overlaid on the sample. Grid orientation was determined with a random number generator.

MLI was determined by the total grid length divided by the number of intercepts. A minimum of 1500 intercepts was counted per lung. Surface area (SA) was then calculated by the equation SA=4V/MLI.

Isotropic growth

The inferred structural changes in the lung during compensatory growth required a modification of conventional nomenclature (Ardila, Horie, & Hildebra.J, 1974). Here, the term “isotropic” growth was applied to the description of alveolar distension or uniform growth; that is, a growth situation in which the statistical average of the rate of growth was identical in all directions.

Cell isolation and bronchoalveolar lavage (BAL)

After a cervical tracheostomy, an olive-tipped catheter was inserted into the distal trachea and secured with a silk suture. Cold PBS (500 ul) was slowly delivered and retrieved through the catheter; the lavage was repeated 7 times. BAL cells were treated with red blood cell lysis buffer (BD Biosciences), washed in 3% serum containing medium, and stored on ice for subsequent analysis.

Tissue versus airspace cells

$CD11b^+$ population from BAL was used for airspace $CD11b^+$ cells. Lung tissue digestion after BAL treatment was processed as described previously (Gibney et al., 2012) $CD11b^+$ population from tissue digestion was used as tissue CD11b+ cells.

Cell counting

BAL-derived cells were counted using a Neubauer hemacytometer (Fisher, Pittsburgh, PA, USA). Dead cells were excluded by trypan blue (Sigma, St Louis, MO, USA). The numbers of $CD11b^+$ cells were calculated by using flow cytometric analysis: ($CD11b^+$ number) = (total BAL cell number) × (% of $CD11b^+$ cells among total cells) / 100.

Immunohistochemistry

Cryostat sections were obtained from lung specimens perfused with O.C.T. compound and snap frozen. After warming the slide to 27°C, the sections were fixed for 10 minutes (2% paraformaldehyde and PBS at pH 7.43). The slides were washed with buffer (PBS, 5% sheep serum, 0.1% azide, 1mM $MgCl_2$, 1mM $CaCl_2$) and blocked with 20% sheep serum, 20% goat serum, 0.1% azide in PBS. The slides were treated with anti-CD11b mAb (PE, rat IgG2b, clone M1/70, BD Bioscience) or isotype control rat IgG2b (PE, clone A95-1, BD Bioscience). The slides were incubated for one hour at 27°C, washed 3 times and mounted with DAPI-containing medium (Vector Labs. Burlingame, CA, USA).

Fluorescence microscopy

The tissue sections were imaged with a Nikon Eclipse TE2000 inverted epifluorescence microscope using Nikon objectives of 20, and 40 linear magnification with infinity correction. An X-Cite™ (Exfo, Vanier, QC, Canada) 120 W metal halide light source and a liquid light guide was used to illuminate the tissue samples. The tri-color excitation and emission filters (Chroma Technology, Bellows Falls, VT, USA) were controlled by a MAC5000 controller (Ludl, Hawthorne, NY, USA) and MetaMorph® software 7.75 (Molecular Devices, Downington, PA,USA). The fluorescence microscopy 14-bit fluorescent images were digitally recorded on a C9100-02 camera (Hamamatsu, Japan), digitally recombined and pseudocolored based on recording wavelength.

Monoclonal antibodies

For flow cytometric lung cell analyses, fluorescein isothiocynate (FITC)-, phycoerythrin (PE)-, allophycocyanin (APC)-, PE-Cy7-conjugated monoclonal antibodies (mAb) were used: anti-CD45 mAb (FITC, rat IgG2b, clone 30-F11, eBioscience), anti-CD11c mAb (PE or APC; hamster IgG, clone N418, eBioscience), anti-CD11b mAb (PE-Cy7, rat IgG2b, clone M1/70, BD Bioscience), anti-Gr-1 mAb (APC, rat IgG2b, clone RB-8C5, eBioscience), anti-Ly6G mAb (biotin, clone 1A8, BD Bioscience), anti-F4/80 mAb (biotin, rat IgG2a, clone BM8, eBioScience), anti-NK1.1 (PE, mouse IgG2a, clone PK136, eBioscience), anti-major histocompatibility complex (MHC) class II mAb (PE-Cy7, Rat IgG2b, clone M5/114.15.2, ebioscience), anti-T1α mAb (PE, hamster IgG, clone eBio8.1.1, eBioscience), anti-CD31 mAb (APC, IgG2a, clone 390, eBioScience), anti-CD11c mAb (PE or APC; hamster IgG, clone N418, eBioScience), isotype control rat IgG2a (biotin, clone eBR2a, eBioscience), isotype control rat IgG2b (FITC, APC or PE, clone A95-1, BD Bioscience), isotype control rat IgG2b (PE-Cy7, clone RTK4530, Biolegend), isotype control hamster IgG (PE, clone HTK888, Biolegend) and isotype control hamster IgG (APC, clone eBio299arm, eBioscience).

Flow cytometry

For standard phenotyping, the cells were incubated with a 5-fold excess of anti-mouse antibodies directly conjugated with FITC, PE, APC, PE-Cy7 or biotin. The cells stained with biotinylated antibodies were washed by FACS buffer (BD Biosciences) and subsequently stained with streptavidin-RPE (Sigma). The cells were analyzed by FACSCanto II (BD, Franklin Lakes NJ, USA) with tri excitation laser (407nm, 488nm and 633nm ex). The data were analyzed by FCS Express 4 software (De Novo Software, Los Angeles, CA, USA). In all analyses, debris were eliminated by gating the alive cell population of Side Scatter (SSC) and Forward Scatter (FSC), and further by gating 7AAD (BD Biosciences)-negative population.

PCR arrays

The commercially available Angiogenesis PCR Array (catalog PAMM-024) and Extracellular Matrix/Adhesion Molecules PCR array (catalog PAMM-013) obtained from SABiosciences (Frederick, MD, USA) was used for all PCR array experiments. Real-time PCR was performed as described previously (Chamoto, Gibney, Ackermann et al., 2012) The standard deviations of the same genes studied on different PCR array plates were uniformly less than 1 Ct. Similarly, the 11 genes common to both arrays demonstrated *Col4a3, Ctgf, Itgav, Itgb3, Mmp2, Mmp9, Pecam1, Thbs1, Thbs2, Trimp1 and Trimp2*.

RNA quality

For the rapid analysis of RNA quantity and quality, all samples were analyzed using the microfluidics-based Agilent 2100 Bioanalyzer (Agilent Technologies, Palo Alto, CA, USA), a chip-based nucleic acid separation system. In most samples, the RNA Pico 6000 LabChip kit (Agilent Technologies) was used. RNA integrity numbers (RIN)(Schroeder et al., 2006) of the RNA samples were uniformly greater than 7.0.

Statistical analysis

Our quantitative PCR assumed that DNA template and/or sampling errors were the same for all amplifications; our internal control replicates indicated that our sample size was sufficiently large that sampling errors were statistically negligible (Stolovitzky & Cecchi, 1996). The exponential phase of the reaction was determined by a statistical threshold (10 standard deviations). Flow cytometry statistical analysis was based on measurements in at least three different mice. The unpaired Student's t-test for samples of unequal variances was

used to calculate statistical significance. The data was expressed as mean ± one standard deviation. The significance level for the sample distribution was defined as $p<.05$.

Results

Lung growth

Growth of the remaining right lung after left pneumonectomy was assessed using both water displacement (Scherle) and insufflation methods. Mean post-pneumonectomy single lung volumes increased 51% (0.78±.04 ml to 1.18±.12 ml) within 21 days to approximate the two lung control volume (1.2±.07 ml; $p = 0.39$). Morphometric measurements of mean linear intercept (MLI) were also performed on a subset of post-pneumonectomy single lungs (N=4 each data point). The relationship of lung volume and MLI permitted the calculation of surface area (Campbell & Tomkeieff, 1952). Using physiologic volume calculations, the post-pneumonectomy lung surface area increased from 22.4×10^3 cm^2/kg to 27.6×10^3 cm^2/kg; that is, an increase in surface area corresponding to the 0.95^{th} power of lung volume (Figure 2A, solid line). In contrast, an increase in lung volume due to alveolar distension alone—that is, inflation without septation—predicted an increase in surface area corresponding to the 0.66^{th} power of lung volume (Figure 2A, dotted line). The difference between observed and predicted surface area was significant ($p < 0.05$). Also consistent with lung growth, there was no significant change in MLI at 4 post-pneumonectomy time points (mean 55.3±2.7 um)(Figure 2B). A comparison of lung histology obtained in control and post-pneumonectomy mice at these time points demonstrated comparable airspace architecture and no apparent inflammation (Figure 2C-F).

$CD11b^+$ cells in the lung

To determine the potential contribution of blood-borne cells to this lung growth, the post-pneumonectomy lungs were analyzed using enzymatic digestion and flow cytometry. In addition to the expected parenchymal cell populations, an unexpectedly high percentage of $CD11b^+$ cells (17%) were identified in the lung between 7 and 14 days after pneumonectomy (Figure 3A, open circles). The CD11b membrane molecule (Mac-1, CR3) is expressed on granulocytes, monocytes (macrophages), dendritic cells, and natural killer cells, but is not expressed on alveolar macrophages, endothelial cells or alveolar epithelial cells (Gonzalez-Juarrero et al., 2003; Springer, Galfre, Secher, & Milstein, 1979). In addition to whole lung analyses, bronchoalveolar lavage (BAL) also demonstrated an increase in the number of airspace $CD11b^+$ cells (Figure 3A, closed circles). The percentage of $CD11b^+$ cells in the post-pneumonectomy airspace was significantly different from sham thoractomy control lungs on day 14 after surgery (Figure 3B; $p<.001$). Based on the kinetics of $CD11b^+$ cell migration, subsequent studies focused on days 7 and 14 after pneumonectomy.

Blood-to-lung migration

The potential contribution of blood-borne cells to the elevated number of $CD11b^+$ cells was investigated using the parabiotic model (wild-type/GFP) of cell migration. Prior to pneumonectomy, parabiotic mice (wild-type/GFP) with complete cross-circulation (Gibney, Chamoto, et al., 2012) demonstrated that only 15.1±3.9% of the tissue cells and 5.0±0.9% of the airspace (BAL) cells were derived from the peripheral blood (GFP^+). In contrast, pneumonectomy resulted in a significant increase in blood-derived lung cells. Within 14 days of pneumonectomy, the total number of GFP^+ cells increased 1.5-fold in the tissue compartment and 26.5- fold in the airspace compartment (Figure 4). Fluorescence confocal microscopy demonstrated co-localization of the GFP marker (indicating an origin in the peripheral blood) and the CD11b membrane molecule in both the interstitial tissue (Figure 4H) and alveolar airspaces (Figure 4I).

Flow cytometry of the GFP^+ migrating cells 14 days after pneumonectomy demonstrated that 64±5% of the entire population of GFP^+ lung cells was $CD11b^+$. In contrast, other cell populations, characterized by the cell surface markers CD31, T1-α, and MHC class II, each comprised 5% or less of the GFP^+ cells. Consistent with previous results (Chamoto, Gibney, Lee, et al., 2012; Lin et al., 2011), thoracotomy alone (without pneumonectomy) had little impact on GFP^+ cell migration 7-14 days after surgery.

$CD11b^+$ cell phenotype

The phenotypic subsets of migratory $CD11b^+$ cells were studied with a separate non-parabiotic analysis of tissue- and BAL-derived leukocytes ($CD45^+$). In the 2 weeks after pneumonectomy, the interstitial compartment (Figure 5A) demonstrated a significant increase in neutrophils ($CD11b^+$, Gr-1^{hi+} cells; $p<.04$) and dendritic cells ($CD11b^+$, $CD11c^+$ cells; $p<.03$); the increase in monocytes ($CD11b^+$, $F4/80^+$ cells) was not significant ($p<0.11$). In contrast, the reciprocal cell composition was noted in the airspace: there was a significant increase in monocytes ($CD11b^+$, $F4/80^+$ cells; $p<.02$) and dendritic cells ($CD11b^+$, $CD11c^+$ cells; $p<.02$), but there was no significant change in the percentage of airspace neutrophils ($CD11b^+$, Gr-1^{hi+} cells; $p<.18$)(Figure 5B). Consistent with previous work (Chamoto, Gibney, Ackermann, et al., 2012), the dominant $CD45^+$, $CD11b^-$ cell population in the airspace was alveolar macrophages.

Dependence of lung growth on $CD11b^+$ cells

To investigate the dependence of lung regeneration on migratory $CD11b^+$ cells, we studied post-pneumonectomy lung growth in mice deficient in the CD18 molecule ($CD18^{-/-}$ mutants) (Mizgerd et al., 1997); that is, a deficiency in the CD11b/CD18 heterodimer (Harlan, 1993). BAL demonstrated very few detectable cells in the $CD18^{-/-}$ post-pneumonectomy airspace (Figure 6A). More notably, the limited migration of leukocytes into the lung was associated with impaired post-pneumonectomy lung growth as reflected by lung weight (Figure 6B, $p<.05$). Also consistent with limited post-pneumonectomy growth, FlexiVent lung mechanics demonstrated that, despite a return to normal lung compliance by day 14, post-pneumonectomy compensatory growth had regained only 61±8% of the lung volume index (ml/kg body weight) compared to 84±9 in age matched wild-type mice ($p<.05$).

Transcriptional profiling of tissue and airspace $CD11b^+$ cells

To demonstrate the gene expression of the $CD11b^+$ cells, and investigate their potential contribution to lung growth, we examined quantitative RT-PCR arrays relevant to lung regeneration. Because the PCR arrays provided a relative measure of gene regulation, we compared the mRNA of tissue and airspace $CD11b^+$ cells on angiogenesis (Figure 7A) and adhesion/extracellular matrix (Figure 7B) arrays. In the angiogenesis arrays, the tissue $CD11b^+$ cells demonstrated increased expression of the *Npr1*, *Tgfb2*, and *Egf genes*; the airspace $CD11b^+$ cells demonstrated increased expression of the *Mmp9*, *Angpt1* and *Il1b genes* (Figure 7A). In the adhesion molecule and extracellular matrix arrays, the tissue $CD11b^+$ cells demonstrated increased gene expression of *Mmp7* (matrilysin), *Adamts2* and *Ecm1*; the airspace $CD11b^+$ cells demonstrated higher gene expression of the selectin genes (*Sele, Sell, Selp*), *Ncam1* as well as *Mmp9* and *Mmp8* (Figure 7B). In each case, the gene expression demonstrated a greater than 4-fold change in mRNA and were statistically significant by t-test comparison of the tissue and airspace $CD11b^+$ cells ($p<.05$).

Discussion

In this report, we investigated the contribution of blood-borne cells to the regenerating adult lung. After murine pneumonectomy, we found that 1) $CD11b^+$ cells were the dominant

blood-borne population migrating into the remaining lung, 2) the migrating $CD11b^+$ cells partitioned into two compartments: interstitial tissue and pulmonary airspace; 3) a genetic deficiency in the CD11b molecule ($CD18^{-/-}$ mutation) was associated with impaired lung growth, and 4) both tissue and airspace $CD11b^+$ cells expressed genes associated with alveolar angiogenesis and ECM remodeling. Together, these data suggest that blood-borne $CD11b^+$ cells represent an accessory cell population capable of contributing to adult lung growth.

Defining regeneration as “the replacement of missing structures following injury” (Morgan, 1901), compensatory lung growth after pneumonectomy is an extraordinary example of mammalian tissue regeneration. After left pneumonectomy, the missing lung tissue is not regrown orthotopically in the left hilum (epimorphosis), but replaced to near-baseline levels by efficient remodeling of the remaining lung. Morphometric studies, including the data presented here, indicate that the increase in lung volume is associated with an increase in both surface area and alveolar number (Fehrenbach et al., 2008). Although the mechanism of regeneration is unclear, the missing alveoli appear to be replaced by a combination of processes including the reorganization of existing tissue elements (morphallaxis) (Konerding et al., 2012), cell proliferation (Lin et al., 2011) and cell migration (Chamoto, Gibney, Lee, et al., 2012).

The goal of our studies was to identify the blood-borne cells potentially contributing to post-pneumonectomy lung growth. Here, we demonstrated that more than 60% of the blood-borne cells migrating into the regenerating lung were $CD11b^+$. The CD11b molecule was an empirically defined marker, but it conveniently identified nearly all of the migratory leukocytes and excluded non-migratory alveolar macrophages (Chamoto, Gibney, Ackermann, et al., 2012). Within the $CD11b^+$ population, most of the cells appeared to be monocytes, dendritic cells ($CD11c^+$) and granulocytes. The distinctive transcriptional signature of the airspace and tissue $CD11b^+$ cells suggested that the physical location of the cells was not random, but reflected unique functional roles in either tissue morphogenesis or host defense.

The relevance of $CD11b^+$ cells to lung regeneration was suggested by the impaired post-pneumonectomy lung growth observed in $CD18^{-/-}$ mutant mice. Expressing very low levels of the CD11b molecule (a hypomorphic mutation analogous to a moderate form of leukocyte adhesion deficiency-1) (Etzioni, Doerschuk, & Harlan, 1999), the $CD18^{-/-}$ mice demonstrated a dramatic decrease in airspace migration and a measurable decrease in lung weight and lung volume 14 days after pneumonectomy. Although the $CD18^{-/-}$ mutation is commonly linked to impairment in the inflammatory phase of wound healing (Sindrilaru et al., 2009), wild-type post-pneumonectomy lung growth is not associated with histologically demonstrable leukocyte inflammation.

In the absence of inflammation, there are several possible, and mutually compatible, functional roles for blood-borne $CD11b^+$ cells in post-pneumonectomy lung growth. First, the appearance of $CD11b^+$ cells in the lung may simply reflect the stochastic migration of monocytes/macrophages. After thoracic surgery in humans, there is an early increase in the number of peripheral blood $CD11b^+$ cells (Hiesmayr et al., 1999). Another possibility is that the primary function of the $CD11b^+$ cells is to regulate, and potentially minimize, inflammation in the airspaces. The enhanced gene transcription of all three members of the selectin family: E-selectin (CD62E, ELAM1), L-selectin (CD62L, LAM1, LECAM1) and P-selectin (CD62P, GMP-140, PADGEM) without detectable surface expression suggests the possibility that these molecules were secreted into the airspace (Vestweber & Blanks, 1999) —a mechanism compatible with the active regulation of neutrophil migration by airspace $CD11b^+$ cells.

A third possibility is that the CD11b$^+$ cells contribute to lung remodeling as "accessory cells" in the process of neoalveolarization. Consistent with this possibility, monocytes and macrophages have been implicated in vascular patterning in embryonic development, as well as angiogenic remodeling in adult tissue repair and tumor growth. In the developing retina (Lobov et al., 2005) and brain (Fantin et al., 2010), monocyte/macrophage ablation results in an incomplete vascular network. The ability of monocytes/macrophages to modulate the development of vascular networks depends, in part, on physical contact (Fantin et al., 2010). In addition to providing guidance clues for proliferating endothelial cells (Squadrito & De Palma, 2011), monocytes/macrophages are essential for modifying the extracellular matrix. In adults, monocyte/macrophages appear to drill holes in the ECM for sprouting capillaries (Moldovan, Goldschmidt-Clermont, Parker-Thornburg, Shapiro, & Kolattukudy, 2000). In tumor models, high macrophage counts correlate with tumor angiogenesis (Leek et al., 1996); depletion experiments result in decreased angiogenesis (De Palma et al., 2005; De Palma, Venneri, Roca, & Naldini, 2003). Here, the evidence for an "accessory cell" role in lung growth was limited to 1) the increased migration of CD11b$^+$ cells coincident with the process of neoalveolarization, 2) impaired lung growth in CD18$^{-/-}$ mice, and 3) the enhanced transcription of genes associated with tissue growth and repair. Because of the limited methods of documenting lung growth function—limited largely to morphometric summary statistics—further insights into the contribution of CD11b$^+$ cells will require a better understanding of the process of neoalveolarization.

Finally, the potential contribution of CD11b$^+$ cells to the regenerative microenvironment highlights the experimental challenges in defining the mechanism of lung growth. The distinct transcriptional profiles of the CD11b$^+$ cells, and their migration into different anatomic compartments, suggests that the CD11b$^+$ cells participate in a complex network of signaling interactions. Our results suggest that traditional experimental manipulations—such as ablation and reconstitution experiments— are unlikely to clarify the relative contribution of blood-borne leukocytes to lung growth. In addition, the design-based morphometry used to assess growth (e.g. mean linear intercept) are too insensitive to detect "accessory" contributions to the regenerative microenvironment. Rather, we anticipate that an understanding of leukocyte contributions to lung growth will require an understanding of the network of intercellular signaling interactions relevant to neoalveolarization (Chamoto et al., 2011; Lin et al., 2011)—the data presented here represents a contribution toward that goal.

Acknowledgments

This work was supported by NIH grants HL75426, HL94567 and HL007734 as well as the Uehara Memorial Foundation and the JSPS Postdoctoral Fellowships for Research Abroad.

Abbreviations

BAL	bronchoalveolar lavage
MLI	mean linear intercept
APC	allophycocyanin
mAb	monoclonal antibodies
RT-PCR	real time-polymerase chain reaction
Ct	cycle threshold
SA	surface area
VL	volume lung

ECM	extracellular matrix
SD	standard deviation
FSC	forward scatter
SSC	side scatter
RIN	RNA integrity number

References

Ardila R, Horie T, Hildebra J. Macroscopic isotropy of lung expansion. Respir Physiol. 1974; 20(2): 105–115.

Bunster E, Meyer RK. An improved method of parabiosis. Anat Rec. 1933; 57:339–343.

Butler J, Loring SH, Patz S, Tsuda A, Yablonskiy DA, Mentzer SJ. Evidence for adult lung growth in humans. N Engl J Med. 2012; 367(3):244–247. [PubMed: 22808959]

Campbell H, Tomkeieff SI. Calculation of the internal surface of a lung. Nature. 1952; 170(4316):117–117. [PubMed: 14957041]

Chamoto, K.; Gibney, B.; Lin, M.; Lee, GS.; Collings-Simpson, D.; Houdek, J., et al. Regulatory network of angiogenesis gene expression during post-pneumonectomy compensatory growth; Paper presented at the American Thoracic Society; Denver, CO. 2011.

Chamoto K, Gibney BC, Ackermann M, Lee GS, Lin M, Konerding MA, et al. Alveolar macrophage dynamics in murine lung regeneration. J Cell Physiol. 2012; 227:3208–3215. [PubMed: 22105735]

Chamoto K, Gibney BC, Lee GS, Lin M, Simpson DC, Voswinckel R, et al. CD34+ progenitor to endothelial cell transition in post-pneumonectomy angiogenesis. Am J Resp Cell Mol Biol. 2012; 46(3):283–289.

De Palma M, Venneri MA, Galli R, Sergi LS, Politi LS, Sampaolesi M, et al. Tie2 identifies a hematopoietic monocytes required for tumor lineage of proangiogenic vessel formation and a mesenchymal population of pericyte progenitors. Cancer Cell. 2005; 8(3):211–226. [PubMed: 16169466]

De Palma M, Venneri MA, Roca C, Naldini L. Targeting exogenous genes to tumor angiogenesis by transplantation of genetically modified hematopoietic stem cells. Nat Med. 2003; 9(6):789–795. [PubMed: 12740570]

Etzioni A, Doerschuk CM, Harlan JM. Of man and mouse: Leukocyte and endothelial adhesion molecule deficiencies. Blood. 1999; 94(10):3281–3288. [PubMed: 10552936]

Fantin A, Vieira JM, Gestri G, Denti L, Schwarz Q, Prykhozhij S, et al. Tissue macrophages act as cellular chaperones for vascular anastomosis downstream of VEGF-mediated endothelial tip cell induction. Blood. 2010; 116(5):829–840. [PubMed: 20404134]

Fehrenbach H, Voswinickel R, Michl V, Mehling T, Fehrenbach A, Seeger W, et al. Neoalveolarisation contributes to compensatory lung growth following pneumonectomy in mice. Eur Respir J. 2008; 31(3):515–522. [PubMed: 18032439]

Gibney B, Chamoto K, Lee GS, Simpson DC, Miele L, Tsuda A, et al. Cross-circulation and cell distribution kinetics in parabiotic mice. J Cell Physiol. 2012; 227:821–828. [PubMed: 21503883]

Gibney B, Houdek J, Lee GS, Ackermann M, Lin M, Simpson DC, et al. Mechanostructural adaptations preceding post-pneumonectomy lung growth. Exp Lung Res. 2012 In press.

Gibney B, Lee GS, Houdek J, Lin M, Chamoto K, Konerding MA, et al. Dynamic determination of oxygenation and lung compliance in murine pneumonectomy. Exp Lung Res. 2011; 37:301–309. [PubMed: 21574875]

Gonzalez-Juarrero M, Shim TS, Kipnis A, Junquieira-Kipnis AP, Orme IM. Dynamics of macrophage cell populations during murine pulmonary tuberculosis. J Immunol. 2003; 171(6):3128–3135. [PubMed: 12960339]

Harlan JM. Leukocyte adhesion deficiency syndrome: Insights into the molecular basis of leukocyte emigration. Clin Immunol Immunopathol. 1993; 67:S16–S24. [PubMed: 8500276]

Hiesmayr MJ, Spittler A, Lassnigg A, Berger R, Laufer G, Kocher A, et al. Alterations in the number of circulating leucocytes, phenotype of monocyte and cytokine production in patients undergoing cardiothoracic surgery. Clin Exp Immunol. 1999; 115(2):315–323. [PubMed: 9933459]

Hsia CCW, Berberich MA, Driscoll B, Laubach VE, Lillehei CW, Massaro C, et al. Mechanisms and limits of induced postnatal lung growth. Am J Respir Crit Care Med. 2004; 170(3):319–343. [PubMed: 15280177]

Kajstura J, Rota M, Hall SR, Hosoda T, D'Amario D, Sanada F, et al. Evidence for human lung stem cells. N Engl J Med. 2011; 364(19):1795–1806. [PubMed: 21561345]

Konerding MA, Gibney BC, Houdek J, Chamoto K, Ackermann M, Lee G, et al. Spatial dependence of alveolar angiogenesis in post-pneumonectomy lung growth. Angiogenesis. 2012; 15:23–32. [PubMed: 21969134]

Leek RD, Lewis CE, Whitehouse R, Greenall M, Clarke J, Harris AL. Association of macrophage infiltration with angiogenesis and prognosis in invasive breast carcinoma. Cancer Res. 1996; 56(20):4625–4629. [PubMed: 8840975]

Lin M, Chamoto K, Gibney B, Lee GS, Collings-Simpson D, Houdek J, et al. Angiogenesis gene expression in murine endothelial cells during post-pneumonectomy lung growth. Resp Res. 2011; 12:98.

Lobov IB, Rao S, Carroll TJ, Vallance JE, Ito M, Ondr JK, et al. WNT7b mediates macrophage-induced programmed cell death in patterning of the vasculature. Nature. 2005; 437(7057):417–421. [PubMed: 16163358]

Matthews KE, Karabeg A, Roberts JM, Saeland S, Dekan G, Epstein MM, et al. Long-term deposition of inhaled antigen in lung resident CD11b(-)CD11c(+) cells. Am J Respir Cell Mol Biol. 2007; 36(4):435–441. [PubMed: 17122367]

Melero-Martin JM, De Obaldia ME, Allen P, Dudley AC, Klagsbrun M, Bischoff J. Host Myeloid Cells Are Necessary for Creating Bioengineered Human Vascular Networks In Vivo. Tissue Eng Part A. 2010; 16(8):2457–2466. [PubMed: 20218762]

Mizgerd JP, Kubo H, Kutkoski GJ, Bhagwan SD, ScharffetterKochanek K, Beaudet AL, et al. Neutrophil emigration in the skin, lungs, and peritoneum: Different requirements for CD11/CD18 revealed by CD18-deficient mice. J Exp Med. 1997; 186(8):1357–1364. [PubMed: 9334375]

Moldovan NI, Goldschmidt-Clermont PJ, Parker-Thornburg J, Shapiro SD, Kolattukudy PE. Contribution of monocytes/macrophages to compensatory neovascularization - The drilling of metalloelastase-positive tunnels in ischemic myocardium. Circ Res. 2000; 87(5):378–384. [PubMed: 10969035]

Morgan, TH. Regeneration. New York: Macmillan; 1901.

Nystul TG, Spradling AC. Breaking out of the mold: diversity within adult stem cells and their niches. Curr Opin Genet Dev. 2006; 16(5):463–468. [PubMed: 16919446]

Ohki M, Ohki Y, Ishihara M, Nishida C, Tashiro Y, Akiyama H, et al. Tissue type plasminogen activator regulates myeloid-cell dependent neoangiogenesis during tissue regeneration. Blood. 2010; 115(21):4302–4312. [PubMed: 20110420]

Scadden DT. The stem-cell niche as an entity of action. Nature. 2006; 441(7097):1075–1079. [PubMed: 16810242]

Schroeder A, Mueller O, Stocker S, Salowsky R, Leiber M, Gassmann M, et al. The RIN: an RNA integrity number for assigning integrity values to RNA measurements. BMC Mol Biol. 2006; 7:1–14. [PubMed: 16412221]

Sindrilaru A, Peters T, Schymeinsky J, Oreshkova T, Wang HL, Gompf A, et al. Wound healing defect of Vav3(-/-) mice due to impaired beta(2)-integrin-dependent macrophage phagocytosis of apoptotic neutrophils. Blood. 2009; 113(21):5266–5276. [PubMed: 19147786]

Springer T, Galfre G, Secher DS, Milstein C. MAC-1 - a macrophage differentiation antigen identified by monoclonal antibody. Eur J Immunol. 1979; 9(4):301–306. [PubMed: 89034]

Squadrito ML, De Palma M. Macrophage regulation of tumor angiogenesis: Implications for cancer therapy. Mol Asp Med. 2011; 32(2):123–145.

Stolovitzky G, Cecchi G. Efficiency of DNA replication in the polymerase chain reaction. Proc Natl Acad Sci U S A. 1996; 93(23):12947–12952. [PubMed: 8917524]

Vestweber D, Blanks JE. Mechanisms that regulate the function of the selectins and their ligands. Physiol Rev. 1999; 79(1):181–213. [PubMed: 9922371]

Yan X, Carbayo JJP, Weibel ER, Hsia CCW. Variation of lung volume after fixation when measured by immersion or Cavalieri method. Am J Physiol Lung Cell Mol Physiol. 2003; 284(1):L242–L245. [PubMed: 12388332]

Highlights

- A wild type/green fluorescent protein parabiotic model demonstrated the migration of blood-borne $CD11b^{+}$ cells during lung regeneration.
- Phenotypic subsets of the $CD11b^{+}$ cells partitioned into the airspace and interstitial tissue.
- A genetic deficiency in the CD11b molecule ($CD18^{-/-}$ mutation) was associated with impaired lung growth.
- The CD11b transcriptional profile was consistent with alveolar angiogenesis and matrix remodeling.

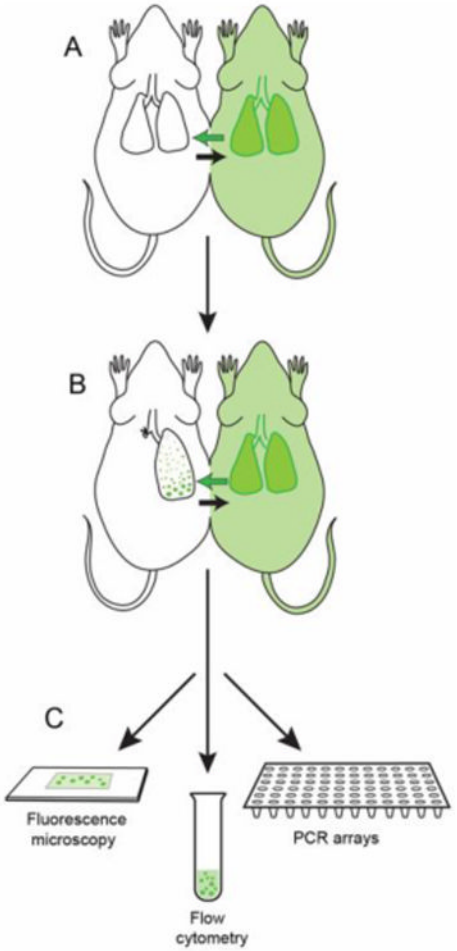

Figure 1.

Schematic of the experimental design involving a left pneumonectomy in the wild-type parabiont of wild-type/GFP$^+$ parabiotic twins (C57/B6). Parabiosis (A) was established for 28 days prior to left pneumonectomy (B). The remaining lung was studied 14 days after pneumonectomy (C) using multi-color fluorescence microscopy, tissue and airspace flow cytometry as well as angiogenesis and ECM PCR arrays.

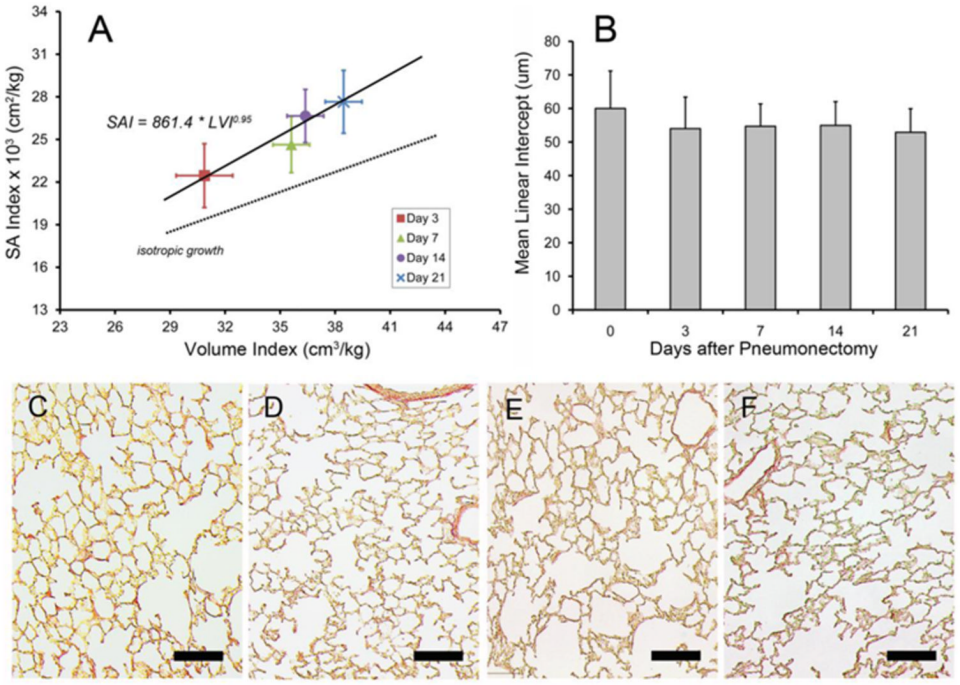

Figure 2.

Morphometric evidence of nonuniform lung growth. A) Measurements of lung volumes and mean linear intercept (MLI) were used to calculate internal surface area using the formula $SA=861.4*V_L^{0.95}$. Both the volume index and surface area index reflect normalization by animal body weight. The geometric mean (N=4 mice each time point) of the aggregate data for days 3, 7, 14 and 21 after pneumonectomy were plotted and a linear trendline calculated ($r^2=0.99$). The expected slope of isotropic lung growth (dotted line) was calculated for comparison. Horizontal error bars reflect 1SD of volume; vertical error bars reflect %SD of MLI on which SA calculations were based. B) MLI data pre-pneumonectomy (day 0) and at 4 experimental time points after pneumonectomy (mean ± SD). C-F) Representative lung histology obtained in control mice (C) and on post-pneumonectomy day 3 (D), day 7 (E), and day 21 (F) are shown. Bar = 100um.

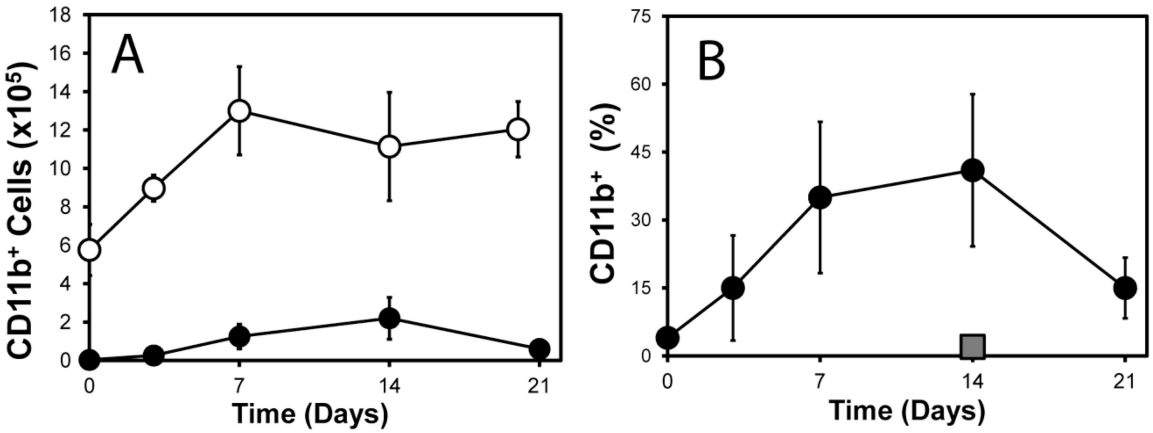

Figure 3.

Kinetics of tissue and airspace $CD11b^+$ cells after pneumonectomy. A) The total number of tissue $CD11b^+$ cells (open circle) and airspace $CD11b^+$ cells (closed circle) were determined on 0, 3, 7, 14, and 21 days after pneumonectomy (each data point, N=4-5 mice). B) The percentage of $CD11b^+$ cells (closed circle) in the airspace was detected on 0, 3, 7, 14, and 21 days after pneumonectomy (each data point, N=4-5 mice). Sham thoracotomy control is shown for comparison (gray square). Error bars reflect the mean ± 1 SD.

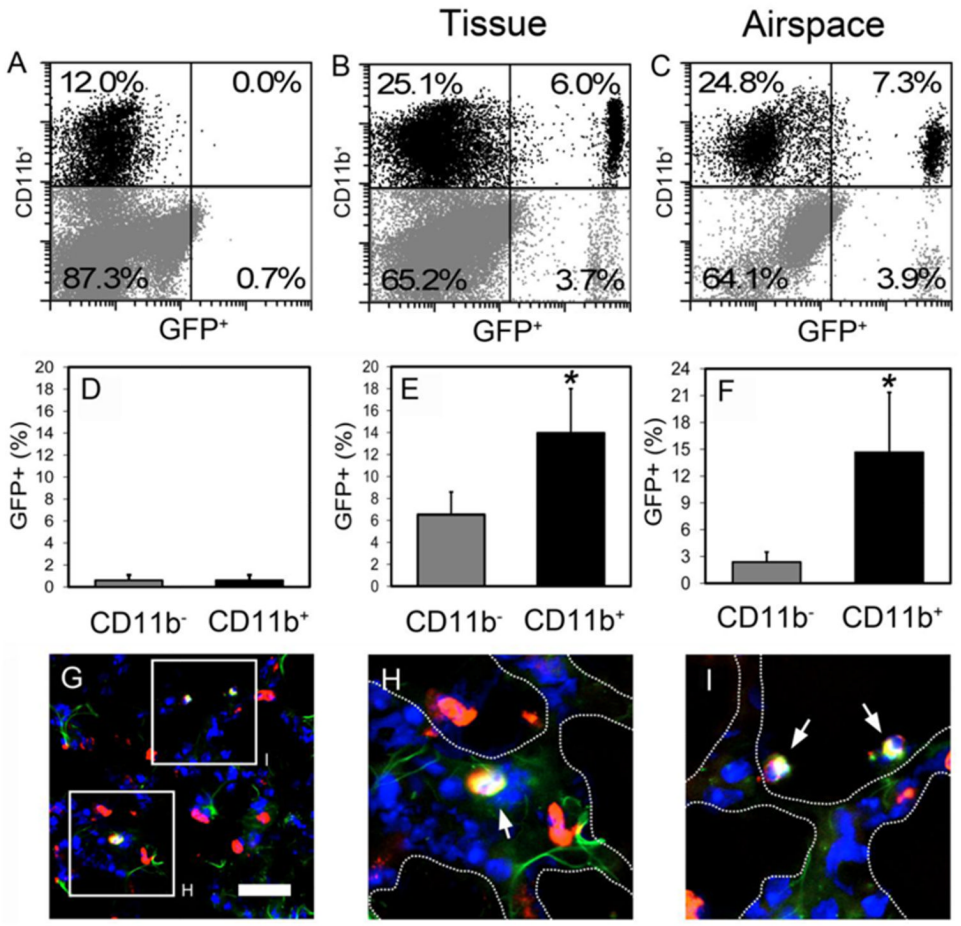

Figure 4.

Localization of GFP$^+$ cells (green) in the lungs of wild-type parabiont (wild-type/GFP parabiotic pair) 14 days after pneumonectomy. A-C) Flow cytometry of tissue cells (B) and BAL-derived cells (C) demonstrated GFP$^+$ cells were present in both the CD11b$^+$ and CD11b$^-$ cell populations. D-I) After gating CD11b$^+$ (black) or CD11b$^-$ cell populations (gray), the frequency of GFP$^+$ cell migration was determined based on wild-type controls (A, D). An average of 6.5± 2.1% among tissue CD11b$^-$ cell and 14.0±4.5% among tissue CD11b$^+$ cells (E), and 2.5±1.1% of airspace CD11b$^-$cells and 14.7±6.7% of airspace CD11b$^+$ cells (F) were blood-borne GFP$^+$ cells ($p<0.05$; N=4 mice, error bars reflect the mean ±1 SD). G-I) Lung fluorescence histologic section stained with anti-CD11b mAb (M1/70, red) and counterstained with the nuclear dye DAPI (blue). Co-localized expression of GFP and CD11b (yellow) was identified in the tissue interstitium (H, arrow) and alveolar airspace (I, arrow).

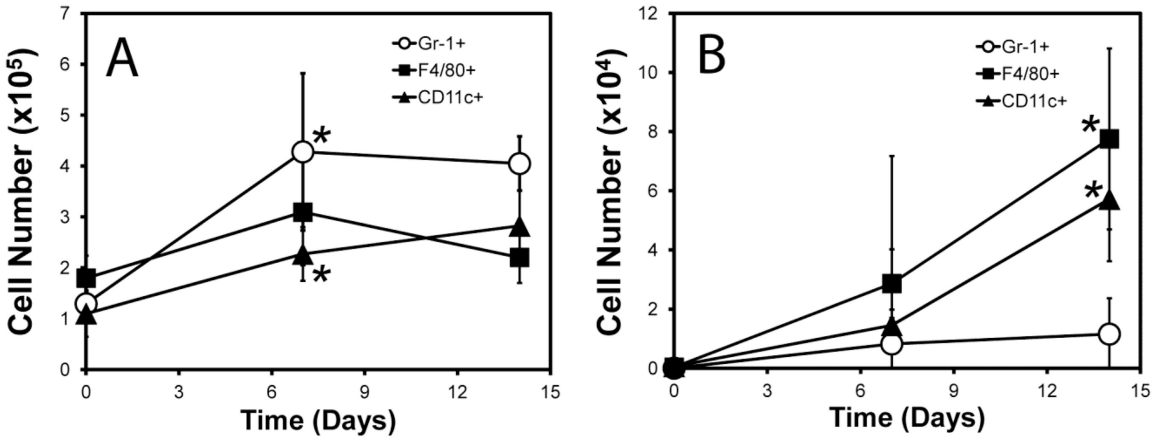

Figure 5.

Subpopulation kinetics of $CD11b^+$ cells days after pneumonectomy. Multiparameter flow cytometry demonstrated the composition of the $CD45^+/CD11b^+$ cells in the interstitial tissue (A) and the airspace (B) after pneumonectomy. A) The interstitial compartment demonstrated a significant increase in neutrophils ($CD11b^+$, $Gr\text{-}1^{hi+}$ cells on day7 compared with day 0; *p<.04) and dendritic cells ($CD11b^+$, $CD11c^+$ cells on day7 compared with day 0; *p<.03), but the increase in monocytes ($CD11b^+$, $F4/80^+$ cells) was not significant (p<0.11). B) The airspace compartment demonstrated a significant increase in monocytes ($CD11b^+$, $F4/80^+$ cells on day14 compared with day0; *p<.02) and dendritic cells ($CD11b^+$, $CD11c^+$ cells on day14 compared with day 0; *p<.02), but there was no significant change in the percentage of neutrophils ($CD11b^+$, $Gr\text{-}1^{hi+}$ cells on day7 and 14 compared with day 0; p<.18).

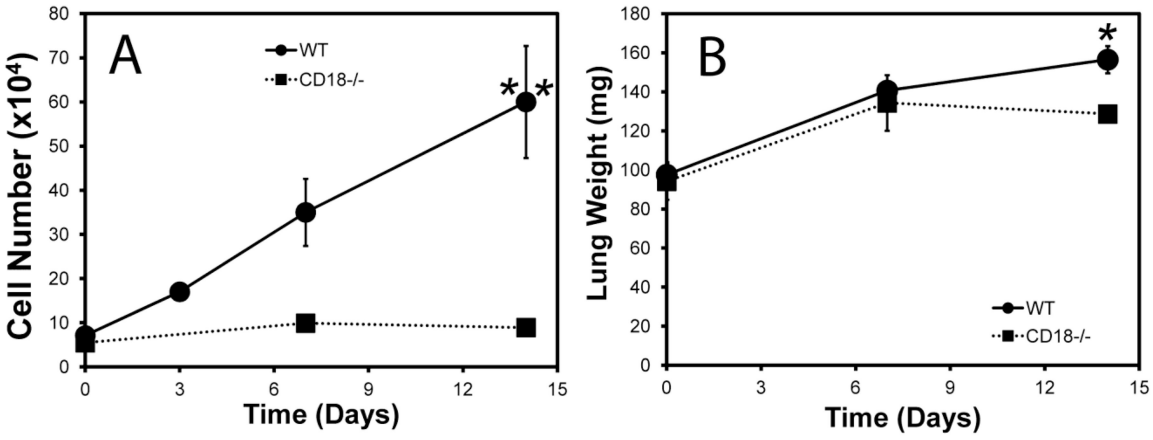

Figure 6.

Impaired lung growth of CD18$^{-/-}$ mice after pneumonectomy. A) Bronchoalveolar lavage of wild-type (WT) and CD18$^{-/-}$ mice after pneumonectomy. Few leukocytes were detected in the lavage fluid of the CD18$^{-/-}$ mice compared to age-matched WT controls (on day 14, **p<.001). B) By 14 days after pneumonectomy, the remaining lung weight of the CD18$^{-/-}$ mice was significantly lower than age-matched WT controls (*p<.05)(N=5 mice per data point).

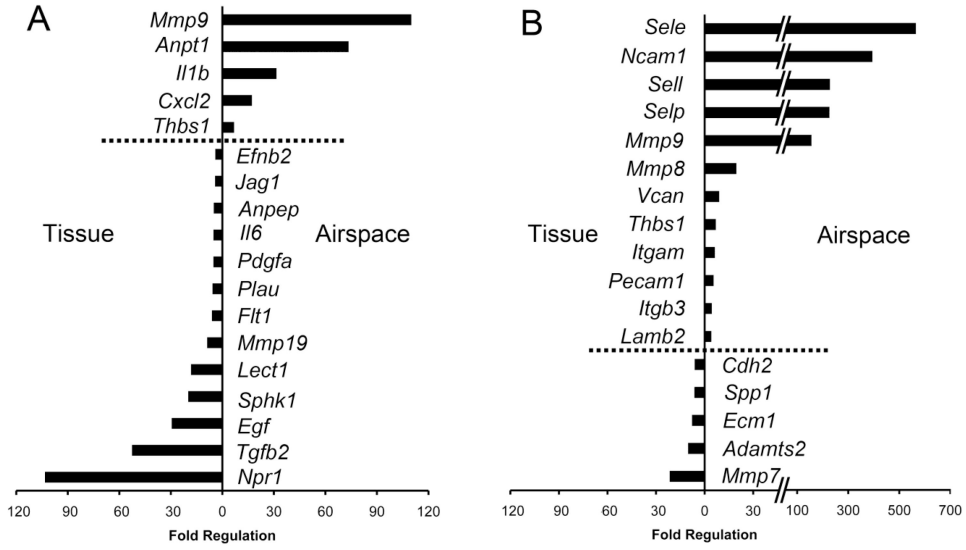

Figure 7.

Expression of angiogenesis-related genes (A), and adhesion/ECM-related genes (B) in tissue and airspace $CD11b^+$ cells 14 days after pneumonectomy. The cell populations were isolated and the transcriptional profile characterized by qRT-PCR. The genes from tissue $CD11b^+$ cells (left side of the panels) and airspace $CD11b^+$ cells (right side of the panels) demonstrating statistically significant expression (fold regulation>4, t-test $p<.05$; comparison between tissue and airspace $CD11b^+$ cells) are shown. Each data point represents triplicate or quadruplicate arrays for each gene; N=3 mice per array.